Materials Science-Poland, 39(4), 2021, pp. 580-598
http://www.materialsscience.pwr.wroc.pl/
DOI: 10.2478/msp-2021-0049

Effect of sea sand and recycled aggregate replacement on fly ash/slag-based geopolymer concrete

Weiwen Li[1], Xinlin Huang[1], Jiali Zhao[1], Yujie Huang[1], Eskinder Desta Shumuye[1,3,*], Xu Yang[2]

[1]Guangdong Provincial Key Laboratory of Durability for Marine Civil Engineering, Shenzhen Durability Centre for Civil Engineering, College of Civil and Transportation Engineering, Shenzhen University, Shenzhen 518060, Guangdong, China

[2]Harbin Institute of Technology at Shenzhen, School of Civil and Environmental Engineering, Shenzhen 518055, Guangdong, China

[3]Department of Construction Technology and Management, Hawassa University Institute of Technology, Hawassa 05, Ethiopia

The purpose of this study is to investigate the impact of recycled aggregate (RA) and sea sand (SS) replacement on fly ash (FA) slag-based geopolymer concrete (GPC). An orthogonal array design is employed to obtain the optimum mix proportions, and geopolymer mixes are prepared using slag percentages of 10%, 20%, and 30% slag in FA/slag-based GPC. Sodium hydroxide (NaOH) solution is prepared at three concentrations (8 mol/L, 12 mol/L, and 16 mol/L). The mechanical properties of the geopolymer mixes are determined based on the tensile strength, compressive strength, flexural strength, and elastic modulus. GPC is prepared using water-binder ratios of 0.3, 0.4, and 0.5 at 0%, 25%, 50%, 75%, and 100% of RA replacement. The results showed that the variation in the RA replacement ratio had little effect on the strength and elastic modulus of sea sand geopolymer concrete (SS–GPC), but it had a significant effect on river sand geopolymer concrete (RS–GPC). The RA replacement ratio also showed a noticeable change in the damage surface of the specimens. In addition, SS hinders the hydration reaction of the geopolymer in the early stage and reduces the early strength of the GPC; however, in the later stages, the effect becomes insignificant.

Keywords: *geopolymer concrete, recycled aggregate, sea sand, mechanical properties, microstructure, fly ash*

1. Introduction

The production of cement requires a large amount of energy and natural resources such as limestone and clay, and the resulting emission of greenhouse gases (e.g., carbon dioxide) and dust causes serious environmental pollution [1, 2]. Geopolymers are a new type of inorganic cementitious material, which has advantages of high early strength, as well as acid and alkali resistance. It is a chain of inorganic polymers, which are synthesized by the condensation polymerization of a mixture of a "precursor" and activator. As the reaction is carried out, the chain is twisted and stacked to form a stable three-dimensional (3D) geopolymer network structure. The "precursor" is mainly industrial by-products such as fly ash (FA) and slag or cementitious materials containing amorphous aluminosilicate such as volcanic ash and metakaolin; the activator is primarily a mixture of silicate solutions [3] and alkali metal hydroxide solutions [4]. At present, research into the material properties, mechanics, and durability of geopolymer concrete (GPC) worldwide has realized some initial achievements, and this area has gradually become a research hotspot in the field of engineering materials.

With the continuous increase in the scale of China's urbanization construction, the demand for aggregates in the construction industry has also increased. The excessive exploitation of river sand (RS) and natural aggregate (NA) will lead to serious ecological problems, while the total amount of sea sand (SS) resources in China's offshore is huge; thus, the mixture of concrete with SS can be regarded as a good method for the comprehensive utilization and sustainable development of resources. However, in practical engineering, although SS is

* E-mail: eskdes@gmail.com

© 2021. This is an open access article distributed under the Creative Commons Attribution-NonCommercial-NoDerivatives 4.0 License. (http://creativecommons.org/licenses/by-nc-nd/4.0/)

less harmful to the concrete itself, a large amount of sulfate and a variety of chlorides present in SS have a corrosive effect on steel bars, resulting in durability problems [5]. In recent decades, scholars worldwide have conducted a series of investigations and research on the material scale (FA [6], calcium silicate [7], and slag [8]), mechanical [6], microstructural [9], and durability [10] properties of sea sand concrete (SSC), which has shown that the properties of concrete mixed with SS after qualified desalination treatment are in line with the specifications. However, the desalination treatment of SS with excessive chloride ion content will lead to a substantial increase in the economic and time costs. In 2010, the total amount of abandoned concrete generated by demolishing old buildings in China was 239 million tons, and this is expected to grow at an average rate of 8% annually [5, 11]. At present, the primary methods of dealing with this construction waste are landfill and accumulation, which is not only labor and freight intensive but also takes up valuable land resources, causing secondary environmental pollution. The vast majority of this construction waste can be recycled and broken up into "recycled aggregate" (RA) after classification. There is no doubt that the economic and environmental benefits will be huge when RA partly or completely replaces NA in the newly produced concrete to prepare "recycled concrete" (RAC). The development of a new composite material having high strength and durability is suggested by researchers Nuaklong et al. [12] and Le et al. [13]. A compressive study was carried out by Nuaklong et al. [12] between the use of GPC containing RA and crushed limestone coarse aggregate. Experimental results for Nuaklong et al. [12] reveal that RAC aggregate can be used as a coarse aggregate in high calcium FA geopolymer with slightly lower compressive strength compared with crushed lime stone coarse aggregate. Furthermore, Le et al. [13], concluded that the use of recycled coarse aggregate (at 100% replacement) with FA-based alkali activated GPC. Recently, synthetic fibers and nanomaterials have gained a lot of popularity due to their ability to enhance the properties of GPC. With that, Nuaklong et al. [14] and Kotop et al. [15] suggested that the incorporation of synthetic fiber and nanomaterials significantly improved the engineering properties of GPC. Past research [16–19] reported that the compressive strength and durability of RAC are generally inferior to natural aggregate concrete (NAC). However, Shi et al. [20] found that, the compressive strength of RA–GPC was higher than that of OPCC. At the same time, Khedmati et al. [21] found that, RA–GPC showed better durability than RA–OPCC.

The main objective of this study is to explore the effect of SS and RA replacement on FA slag-based GPC. Based on the optimum mix proportions summarized by the L9 (3^3) orthogonal array method [22, 23], SS–RA–GPC was prepared. The studied parameters included two types of sand (SS or RS) and the RA replacement ratio (0%, 25%, 50%, 75%, and 100%), which enabled the study of the effect of SS and RA on the mechanical properties of GPC. The microstructures and hydration products of the prepared specimens were analyzed using scanning electron microscopy (SEM).

2. Experimental investigation

2.1. Materials

The recycled coarse aggregate crushed and screened from the old grade C25–C30 concrete building and natural granite aggregate were also used as a reference, as shown in Figure 1. The density, fineness modulus, shell content, and chloride ion content of SS were determined according to JGJ/52-2006. The materials used are the V1500-I type FA, V500 (S95) type slag, and P.O. 42.5 cement, for which the detailed physical and chemical compositions are given in Tables 1 and 2. The geopolymer alkaline activator was formed by a mixture of NaOH and Na_2SiO_4 solutions with a mass ratio of 1:2.5. This ratio of 1:1.5 has also been widely used by previous researchers as an optimum value [24–26]. Relevant performance indices of the materials are shown in Tables 3 and 4.

2.2. Experimental design

The mechanical and microstructural properties of GPC depend on different mixing parameters, such as the alkali activator concentration and the

Table 1. Basic performance index of aggregate

Aggregate type	Particle size (mm)	Apparent density (kg/m^3)	Bulk density (kg/m^3)	Water absorption (%)	Crushing index (%)
Natural coarse aggregate	5–20	2,780	1,420	0.15	9.22
Recycled coarse aggregate	5–20	2,250	1,380	6.07	15.97

*The apparent density, bulk density, water absorption, and crushing index are determined in accordance with the specification "Gravel and Crushed Stone for Construction" (GB/T 14685-2011).

Table 2. Main chemical composition of FA and slag

Combined components	Loss on ignition (%)	CaO (%)	SiO_2 (%)	Al_2O_3 (%)	MgO (%)	Fe_2O_3 (%)	SO_3 (%)
FA	3.79	6.66	42.34	25.84	1.17	5.46	0.95
Slag	0.34	34.45	27.46	16.24	8.46	0.42	0.81

FA, fly ash

Table 3. NaOH solution formulation

Molarity	Proportion of NaOH solids (wt.%)	Proportion of distilled water (wt.%)
8 mol/L	25.1	74.9
12 mol/L	32.43	67.57
16 mol/L	39.02	60.98

Table 4. Chemical properties of sodium silicate solution

Modulus	Baume degree (Be)	Na_2O (wt.%)	SiO_2 (wt.%)	H_2O (wt.%)
3.12	40	8.5	26.5	65

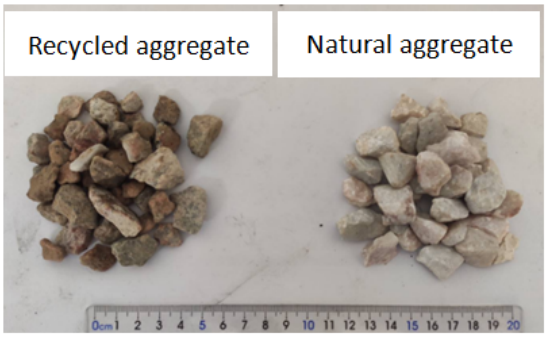

(A)

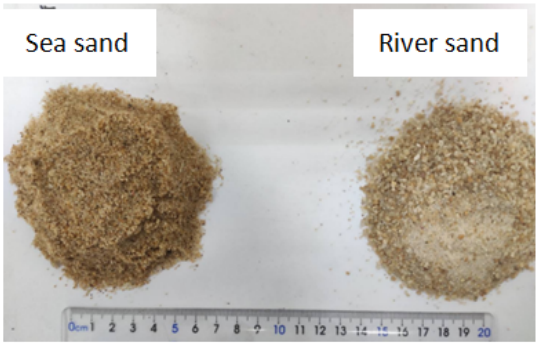

(B)

Fig. 1. Aggregate used in this research. **(A)** Coarse aggregate. **(B)** Fine aggregate

ratio of FA to slag. To determine the optimum mix proportion of the slurry and to optimize the strength and workability of the GPC, an orthogonal array design is implemented. Based on the recent and available literature [24–26], three main factors that alter the strength and workability of geopolymer were identified as the RA replacement ratio, NaOH concentration, and binder to activator ratio. Geopolymer mixes were prepared using 10%, 20%, and 30% slag ratios in FA/slag-based GPC. The alkaline activator used was a mixture of sodium silicate (Na_2SiO_4) and sodium hydroxide (NaOH) at three concentrations (8 mol/L, 12 mol/L, and 16 mol/L). The ratio selected was based on the findings in the literature [24–26], which gave the best results of GPC. Moreover, water-binder ratios of

Table 5. Mixture proportion of orthogonal test (kg/m^3)

Test number	FA	Slag	SS	NA	NaOH solution	Na_2SiO_3 solution	Slag content (%)	Water-binder ratio	NaOH solution concentration
1	499	55	449	1,047	70	175	10	0.3	8 mol/L
2	322	81	495	1,153	70	175	20	0.4	12 mol/L
3	219	94	522	1,215	70	175	30	0.5	16 mol/L
4	266	66	516	1,202	70	175	20	0.5	8 mol/L
5	376	161	454	1,058	70	175	30	0.3	12 mol/L
6	352	39	498	1,160	70	175	10	0.4	16 mol/L
7	291	125	491	1,144	70	175	30	0.4	8 mol/L
8	290	32	519	1,209	70	175	10	0.5	12 mol/L
9	417	104	459	1,070	70	175	20	0.3	16 mol/L

*Water-binder ratio refers to the sum of water contained in NaOH solution and Na_2SiO_3 solution, except the solute, divided by the value of the sum of the FA and slag.

*The sum of the masses of FA, slag, fine aggregate, and coarse aggregate of all groups is the same.

FA, fly ash; NA, natural aggregate; SS, sea sand.

Table 6. Mixture proportions of paste and mortar (kg/m^3)

No.	FA	Slag	SS	RS	NaOH solution	Na_2SiO_3 solution
Seawater paste	840	360	0	0	156*	391
DWP	840	360	0	0	156	391
SSM	840	360	600	0	156	391
RSM	840	360	0	600	156	391

*NaOH solution in the group was prepared with seawater, while the others were prepared with distilled water.

DWP, distilled water paste; FA, fly ash; RSM, river sand mortar; SS, sea sand; SSM, sea sand mortar.

0.3, 0.4, and 0.5 at 0%, 25%, 50%, 75%, and 100% artificial aggregate replacement with two different types of sand (SS and RS) were used to prepare the GPC. A similar replacement ratio has also been adopted in the following literature [12, 20]. Based on the optimum mix proportions, geopolymer paste (GPP) and geopolymer mortar (GPM) were prepared to study the effect of seawater and SS on GPP and GPM without coarse aggregates.

2.3. Specimen preparation

FA, slag, and aggregate were first dry mixed in a 100-L mixer for at least 2 min to ensure that all aggregates were coated with the powder mix. Then, the premixed alkali solution was blended into the dry mixture and mixed for approximately 3–4 min. Then, the composite paste/mortar/concrete was poured into 100 mm × 100 mm × 100 mm cube molds and 100 mm (diameter) × 200 mm (height) cylindrical molds, and finally, it was vibrated for 1–2 min using a vibrating table. Thereafter, the samples were demolded after 24 h and cured in a standard curing room until testing.

After obtaining the optimal mix designs, GPP, GPM, and GPC were cast in a similar manner. GPP and CPM were cast into 70.7 mm × 70.7 mm × 70.7 mm cube molds, while GPC was cast into 100 mm × 100 mm × 100 mm cube molds,

Table 7. Mixture proportions of two-factor test (kg/m^3)

NO.	FA	Slag	Sand	NA	RA	NaOH solution	Na_2SiO_3 solution	RA replacement rate	Type of sand	Combined components
SG-0	375.7	161.1	454.4	1,058.7	0	70	175	0	SS	Geopolymer
SG-25	375.7	161.1	454.4	794.1	264.7	70	175	25%	SS	Geopolymer
SG-50	375.7	161.1	454.4	529.4	529.4	70	175	50%	SS	Geopolymer
SG-75	375.7	161.1	454.4	264.7	794.1	70	175	75%	SS	Geopolymer
SG-100	375.7	161.1	454.4	0	1,058.7	70	175	100%	SS	Geopolymer
RG-0	375.7	161.1	454.4	1,058.8	0	70	175	0	RS	Geopolymer
RG-50	375.7	161.1	454.4	529.4	529.4	70	175	50%	RS	Geopolymer
RG-100	375.7	161.1	454.4	0	1,058.8	70	175	100%	RS	Geopolymer
	Portland Cement					Distilled water				
SPC-100	536.8		454.4	0	1,058.8	161.1		100%	SS	Portland cement
RPC-100	536.8		454.4	0	1,058.8	161.1		100%	RS	Portland cement

*The mass of Portland cement is equal to the sum of the mass of FA and slag; the mass of water is equal to the sum of the mass of water in NaOH solution and Na_2SiO_4 solution.

*S stands for sea sand; R stands for river sand; G stands for geopolymer; PC stands for ordinary Portland cement; the last number represents the RA replacement ratio.

FA, fly ash; NA, natural aggregate; RA, recycled aggregate; RS, river sand; SS, sea sand.

100 mm (diameter) × 200 mm (height) cylindrical molds and 100 mm × 100 mm × 400 mm prism molds. The OPCC was made in a manner that was similar to that of the GPC samples.

2.3.1. Slurry proportion test

The specific settings of the L9 (3^3) orthogonal test are listed in Table 5.

2.3.2. Paste and mortar strength test

The mix designs for the GPC employed in this study are listed in Table 6.

2.3.3. Mechanical property test for GPC

In this study, 10 concrete mixes were designed to investigate the mechanical properties of GPC. The other eight mixes were designed for GPC, and two for OPCC, and were prepared by either partially or completely replacing NA with RA. The mix proportions of the designed geopolymer mixes are listed in Table 7.

2.4. Test methods

2.4.1. Workability test

The flowability of GPC was accessed by performing a slump test, which was conducted according to the "Standard for Performance Test Method of Ordinary Concrete Mixture" (GB/T 50080-2016). The inner core of the slump mold has a height of 30 mm, a top diameter of 100 mm, and a bottom diameter of 200 mm.

2.4.2. Test for mechanical properties

The cube compressive test and splitting tensile strength test were evaluated using an MTS YAW4206 200-ton electro-hydraulic servo pressure testing machine following the "Standard for Testing Methods of Mechanical Properties of Ordinary Concrete" (GB/T 50081-2016), with loading rates of 0.6 MPa/s and 0.06 MPa/s, respectively. The flexural strength test was conducted on an MTS C64.305 hydraulic servo universal tension and compression testing machine. According to the Standard for Testing Methods of Mechanical Prop-

Table 8. Average values of various factors in orthogonal test

Variables and grades	3 days compressive strength /MPa	28 days compressive strength /MPa	28 days splitting tensile strength /MPa	Cylinder compressive strength /MPa	Elastic modulus /GPa	Slump /mm	Poisson's ratio
A1	10.28	21.05	1.21	17.55	9.20	235	0.21
A2	15.38	29.03	1.36	27.07	11.20	237	0.23
A3	15.41	29.89	1.53	22.53	9.50	230	0.18
B1	8.29	19.09	1.21	17.12	9.03	231	0.22
B2	14.25	27.75	1.39	21.65	10.30	236	0.18
B3	18.54	33.14	1.50	28.38	10.57	235	0.22
C1	19.32	35.92	1.67	29.34	13.57	208	0.15
C2	12.29	24.40	1.37	22.90	9.50	239	0.24
C3	9.47	19.65	1.06	14.91	6.83	256	0.24

*A stands for the NaOH solution concentration, A1 = 8 mol/L, A2 = 12 mol/L, A3 = 16 mol/L; B stands for the slag content, B1 = 10%, B2 = 20%, B3 = 30%; C stands for the water-binder ratio, C1 = 0.3, C2 = 0.4, C3 = 0.5.

erties of Ordinary Concrete (GB/T 50081-2016), a four-point flexural strength test was adopted with a loading rate of 0.06 MPa/s. The cylinder strength and elastic modulus (E_c) tests were conducted on an MTS YAW6306 300-t hydraulic testing machine according to ASTM C469/C469M – 14 [27], with a loading rate of 0.18 mm/min. The cylindrical samples were ground flat at both ends before testing. Four linear displacement sensors (LVDTs) and two strain gauges were used to measure the longitudinal and transverse strains of the specimens, and a SIR-IUS series 16 channel acquisition instrument was used for data collection with a sampling frequency of 1 Hz. Using Eq. (1) [25, 26] and Eq. (2) [26], the E_c and Poisson's ratio (μ) values were taken as the average of the results obtained in the subsequent loadings:

$$E_c = \frac{s_2 - s_1}{\varepsilon_2 - 0.000050} \quad (1)$$

where E_c is the chord modulus of elasticity in GPa, s_2 is the stress corresponding to 40% of the ultimate load in MPa, s_1 is the stress corresponding to a longitudinal strain of 0.00005 in MPa, and ε_2 is the longitudinal strain corresponding to s_2:

$$\mu = \frac{\varepsilon_{t2} - \varepsilon_{t1}}{\varepsilon_2 - 0.000050} \quad (2)$$

where μ is the Poisson's ratio, ε_{t2} is the transverse strain in the middle of the specimen corresponding to 40% of the ultimate load, ε_{t1} is the transverse strain in the middle of the specimen corresponding to a longitudinal strain of 0.00005, and ε_{t2} is the longitudinal strain corresponding to 40% of ultimate load.

2.4.3. Microstructure analysis

To observe the microstructure of the GPC, small fragments were carefully extracted from the selected specimens using a rubber hammer. SEM images were taken using a Quanta TM-250 FEG at 28 days. After drying, each sample was coated with a platinum layer to prevent charge collection on the surface.

3. Discussion and analysis

3.1. Orthogonal results

The slump test, cube compressive strength test at 3 days and 28 days, cube splitting tensile strength test, and cylinder compressive strength test at 28 days were carried out on nine groups of specimens. To compare the influence of individual factors on the test results, the test results were pro-

cessed and regrouped; these have been presented in Table 8. The mean value of the 3 days compressive strength of groups 1, 4, and 7 were used to represent the 3 days compressive strength when the NaOH solution concentration was 8 mol/L (A1 in Table 8). Similarly, the mean values of groups 2, 5, and 8, and those of groups 3, 6, and 9 represent the 3 days compressive strength when the NaOH solution concentration was 12 mol/L (A2 in Table 8) and 16 mol/L (A3 in Table 8). The results of the slag content (B in Table 8) and water-binder ratio (C in Table 8) were calculated according to the above method and are recorded in Table 8.

3.2. Effects of different factors on mechanical properties of GPP

The influences of various factors on the mechanical properties of GPC are shown in Figures 2–6. It can be seen that the NaOH solution concentration and slag content have little influence on the slump and Poisson's ratio values of GPC, whereas the influence of the water-binder ratio is significant. The NaOH solution concentration, slag content, and water-binder ratio considerably impact the compressive strength and elastic modulus, but the influence law and mechanism are not exactly the same. Moreover, as the NaOH solution concentration and slag content increased and the water-binder ratio decreased, the splitting tensile strength increased.

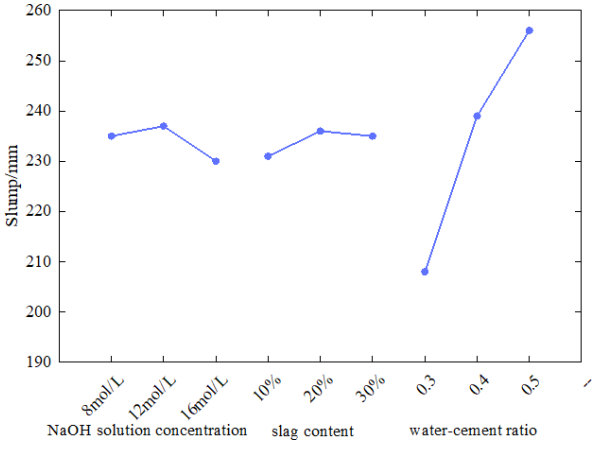

Fig. 2. Factors affecting slump

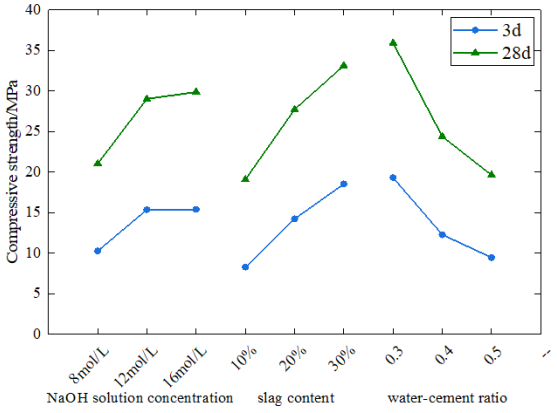

Fig. 3. Factors affecting compressive strength

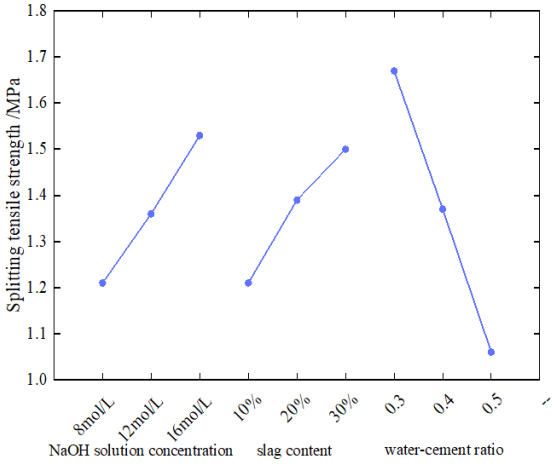

Fig. 4. Factors affecting splitting tensile strength

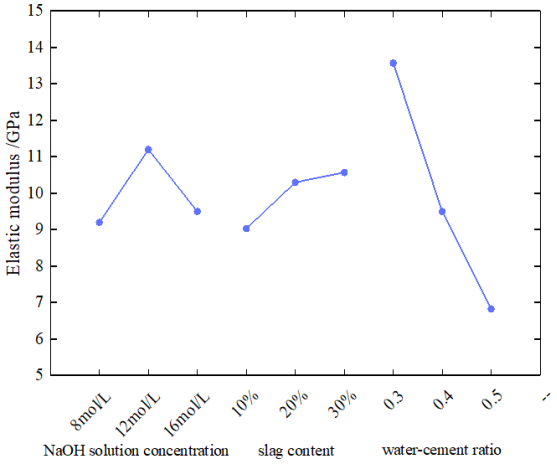

Fig. 5. Factors affecting elastic modulus

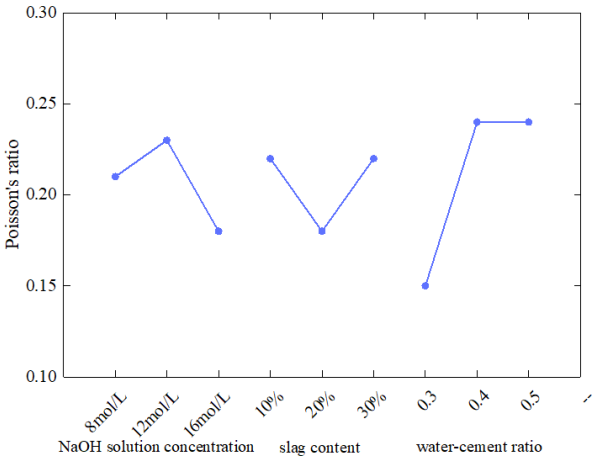

Fig. 6. Factors affecting Poisson's ratio

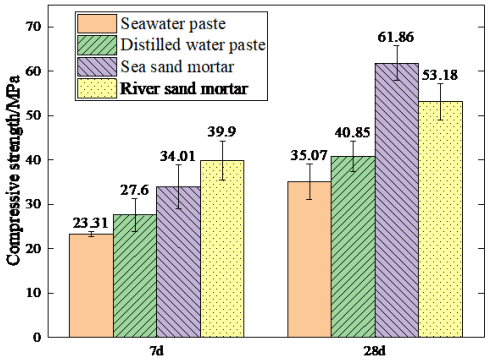

Fig. 7. Compressive strength of paste and mortar

3.3. Optimum mix design

The results of the orthogonal analysis presented above and the results of Xie et al. [26] and Nuaklong et al. [28] can be used to propose optimum mix proportions, that is, a 12 mol/L NaOH solution concentration, 30% slag content, and 0.3 water-binder ratio.

3.4. Strength test results of paste and mortar

Figure 7 shows the results obtained for each group. At 7 days, the compressive strengths of seawater paste (SWP) and sea sand mortar (SSM) were 15.8% and 14.7% lower than those of distilled water paste (DWP) and river sand mortar (RSM), respectively, indicating that seawater and SS reduced the early strength of the geopolymer slurry. At 28 days, the compressive strength of SWP was 14.1% lower than that of DWP, but the compressive strength of SSM was 16.3% higher than that of RSM. This may be because the chloride ions in seawater and SS reduced the pH value of the slurry in the early stage, which hinders the hydration reaction of the geopolymer, and then reduced the early compressive strength of the specimens. However, this hindering effect would fail in the later stages, and the strength would be improved.

4. Effect of RA and SS on mechanical properties of GPC

4.1. Failure mode

Figure 8A–8E shows the failure modes corresponding to sea sand geopolymer concrete (SS–GPC) with RA replacement ratios of 0%, 25%, 50%, 75%, and 100% at 28 days, respectively, and Figure 8F corresponds to SS-OPCC with RA replacement ratios of 100%, where each photo is the most representative specimen selected from the three specimens in each group. As can be seen from Figure 8, all of the specimens were destroyed because of a long crack running through the top and bottom of the specimens. Compared with SS-OPCC, there were more fine cracks near the main crack of the SS–GPC. The strength of NA is higher than that of RA; therefore, when the crack develops to aggregate, it bypasses the NA but directly penetrates the RA (as shown in Figure 9). As a result, the failure surface of the specimen becomes flatter as the RA replacement ratio increases.

Figure 10A–10C, respectively, shows the failure modes corresponding to river sand geopolymer concrete (RS–GPC) with RA replacement ratios of 0%, 50%, and 100% at 28 days, and Figure 10D corresponds to the RS-OPCC with an RA replacement ratio of 100%. The failure mode of RS–GPC is similar to that of SS–GPC with an increase in the replacement ratio. Compared with GPC (Figure 10C), the cracks of the OPCC specimens (Figure 10D) are wider.

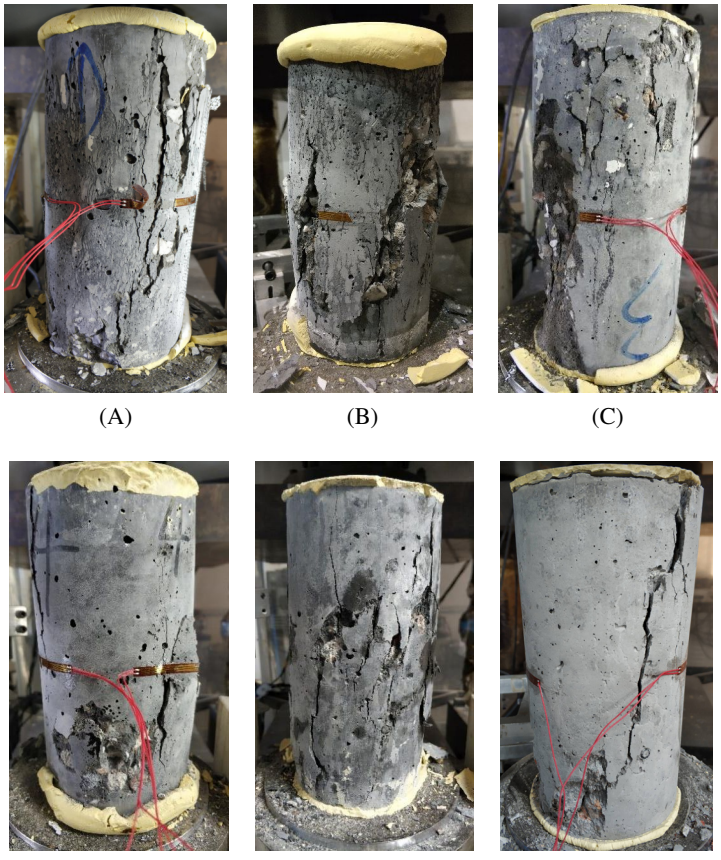

Fig. 8. Failure mode of the SS group. **(A)** SG-0, **(B)** SG-25, **(C)** SG-50, **(D)** SG-75, **(E)** SG-100, **(F)** SPC-100. SS, sea sand

Fig. 9. Fracture surface of specimens. **(A)** Fracture surface of NA, **(B)** Fracture surface of RA. NA, natural aggregate; RA, recycled aggregate

4.2. Flowability

It can be clearly seen from Table 9 that the slump of the GPC is higher than that of the OPCC, indicating that it is a high-fluidity concrete and has better working performance. In addition, the slump of SS–GPC is slightly higher than that of RS–GPC, because SS has a more rounded appearance with fewer edges and corners, as well as a smaller fineness modulus, resulting in greater slurry flowability. Simultaneously, the slump in all groups increased with an increase in the RA replacement ratio. Because RA reached the saturated surface dry (SSD) state before pouring, a small portion of water in the aggregate cracks was released during mixing, which is equivalent to increasing the water-binder ratio [29, 30]. However, many edges and corners of the RA are polished during the manufacturing pro-

(A) (B) (C) (D)

Fig. 10. Failure mode of RS group. **(A)** RG-0, **(B)** RG-50, **(C)** RG-100, **(D)** RPC-100. RS, river sand

Table 9. Test results of two-factor test

NO.	Compressive strength /MPa		Flexural strength /MPa		Splitting tensile strength /MPa		Elastic modulus /GPa		Poisson's ratio		Slump
	7 days	28 days	7 days	28 days	7 days	28 days	7 days	28 days	7 days	28 days	
SG-0	44.92	61.67	2.98	4.13	1.24	1.73	12.6	20.3	0.25	0.21	240
SG-25	43.24	60.10	3.07	3.92	1.26	1.65	12.8	20.5	0.19	0.23	250
SG-50	43.92	61.97	3.13	3.95	1.33	1.58	14.0	20.7	0.16	0.17	254
SG-75	42.67	60.43	3.11	3.81	1.30	1.52	12.5	18.8	0.19	0.21	255
SG-100	42.64	54.80	3.08	3.70	1.31	1.44	13.9	18.1	0.13	0.30	260
RG-0	55.79	66.60	3.60	4.47	1.63	1.73	15.6	23.8	0.19	0.30	235
RG-50	49.89	57.83	2.65	2.95	1.35	1.50	8.8	17.4	0.20	0.30	245
RG-100	44.94	49.50	2.34	2.53	1.10	1.18	6.6	11.1	0.25	0.22	250
SPC-100	38.88	44.23	3.87	4.24	1.33	1.50	24.1	25.9	0.24	0.13	115
RPC-100	30.74	35.93	3.02	3.53	1.33	1.28	23.9	25.1	0.09	0.19	110

cess, enabling the slurry to flow more easily over the surface of RA, resulting in an increased slump.

4.3. Compressive strength f_{cu}

In Figure 11, it can be seen that the cube compressive strength (f_{cu}) of SS–GPC (SG-0, SG-25, SG-50, SG-75, and SG-100) remains relatively stable with an increase in the RA replacement ratio, while the influence of the RA replacement ratio on the compressive strength of SS–GPC at 28 days is more significant than that at 7 days (13.1% and 5.3% difference between the maximum and the minimum, respectively). Simultaneously, the compressive strength of SS–GPC was lower than that of RS–GPC at 7 days. In contrast, the compressive strength of RS–GPC (RG-0, RG-50, and RG-100) exhibited a considerable regular downward trend with the increase in the RA replacement ratio, which is consistent with the experimental phenomena of Xie et al. [31] and Shaikh et al. [32]. In addition, the decline was greater at 28 days than that at 7 days. The strength of the SS–GPC slurry was lower than aggregate at 7 days, owing to an insufficient hydration reaction. Then, the specimens had started to become damaged from the slurry (Figure 12). As the reaction proceeded, the

strength of the SS–GPC slurry exceeded that of RA at 28 days. When the RA replacement ratio increased, the weak part gradually transferred from slurry to RA (Figure 13). In contrast, the strength of RS–GPC exceeds that of RA, so the specimens begin to be damaged from the interface transportation zone (ITZ) or RA (Figure 14). During the preparation of RA, a large number of microcracks are generated, and some old mortar with low strength was attached, resulting in poor quality of RA compared with NA. At the same time, the ITZ between the old mortar and old aggregate in RA was conducive to the more rapid development of cracks, thus reducing the bearing capacity of the specimens [33, 34].

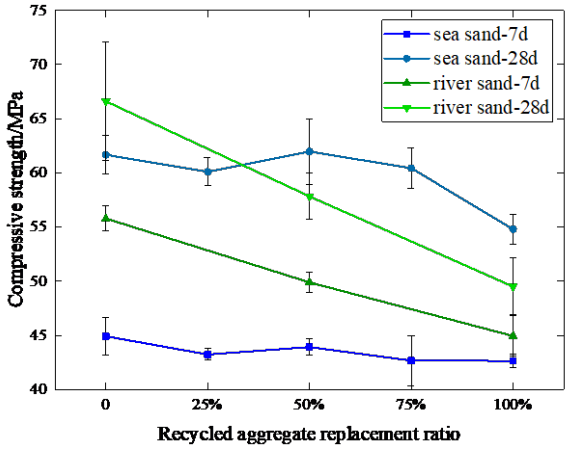

Fig. 11. Influence of RA replacement ratio and sand types on compressive strength. RA, recycled aggregate

Similar to the conclusions made by many other scholars, the compressive strength of SG-0 is lower than that of RG-0, and this is mainly because the fineness modulus of SS is smaller; that is, the specific surface area is larger, reducing the amount of slurry per unit surface area, thus reducing the concrete strength [35–37]. However, the 28-day compressive strength of SS–GPC was higher than that of RS–GPC when the RA replacement ratio was high (>50%). According to the mortar test, the strength of SSM was lower at 7 days but higher at 28 days compared with that of RSM (Figure 7), which indicated that SS improved the hydration reaction in the later stage, thus improving the bond-

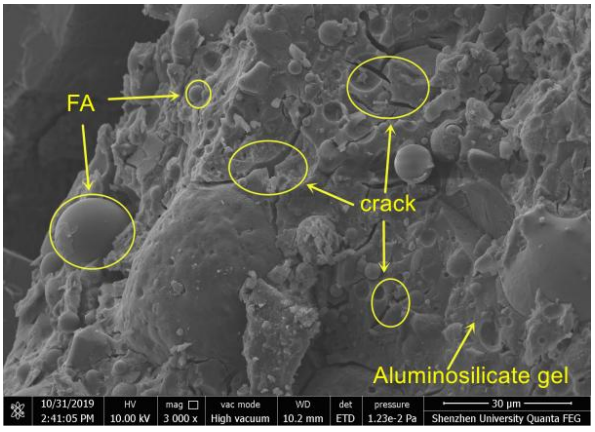

(A)

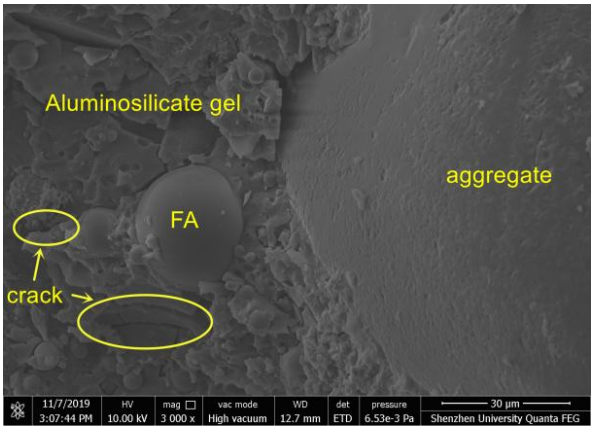

(B)

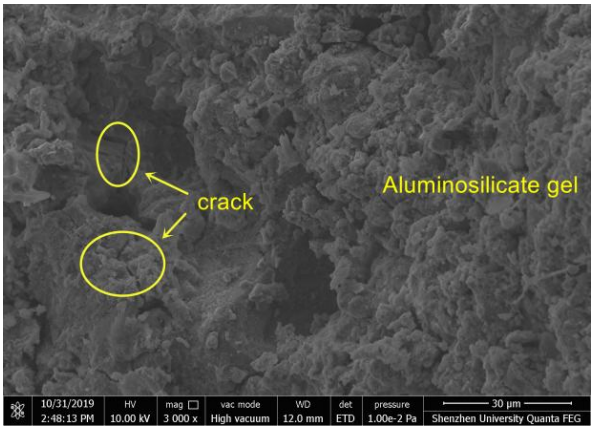

(C)

Fig. 12. SEM photos of SS group at 7 days. **(A)** SG-0, **(B)** SG-50, **(C)** SG-100. SEM, scanning electron microscopy. SS, sea sand

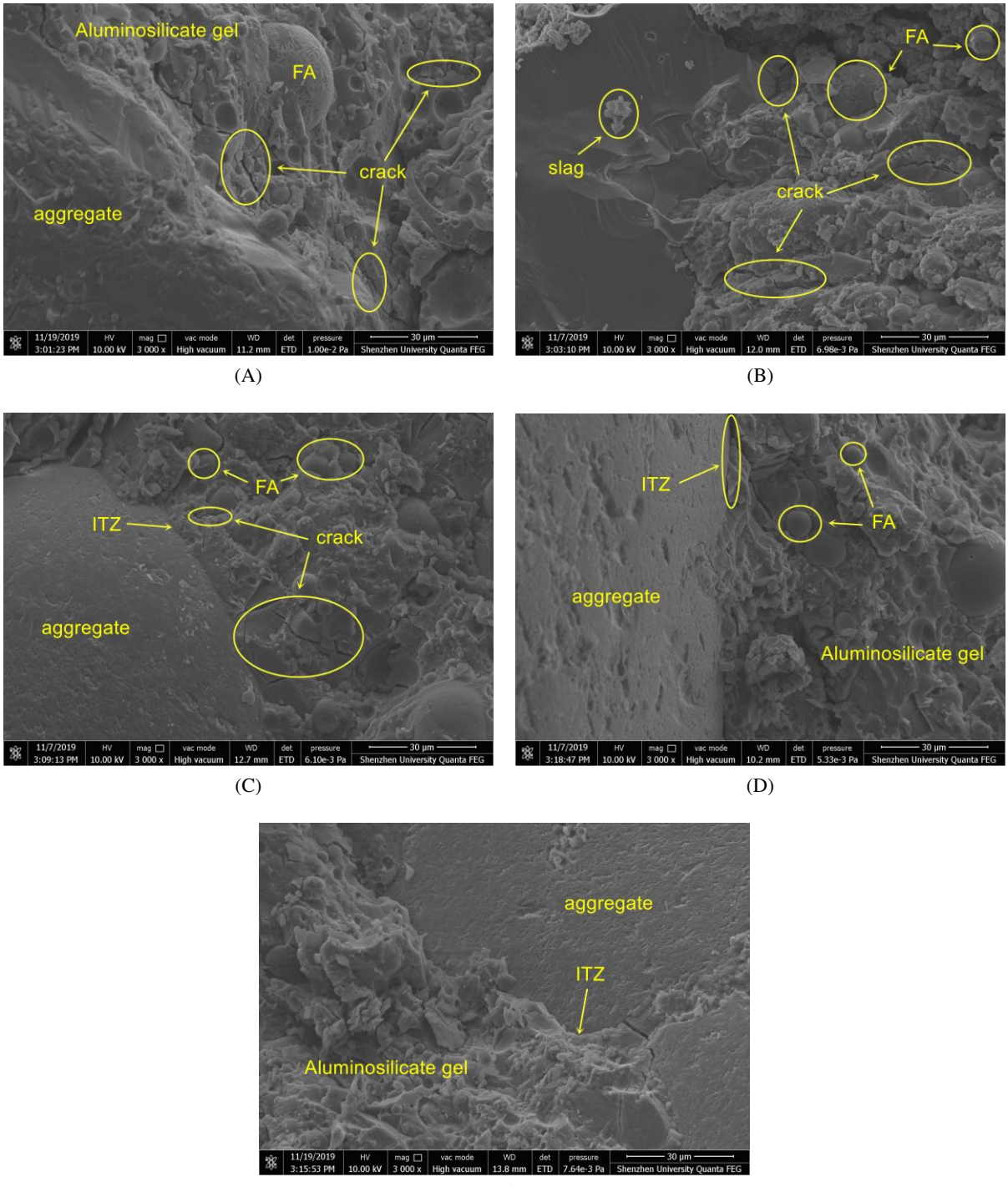

Fig. 13. SEM photos of SS group at 28 days. **(A)** SG-0, **(B)** SG-25, **(C)** SG-50, **(D)** SG-75, **(E)** SG-100. FA, fly ash; ITZ, interface transportation zone; SEM, scanning electron microscopy; SS, sea sand

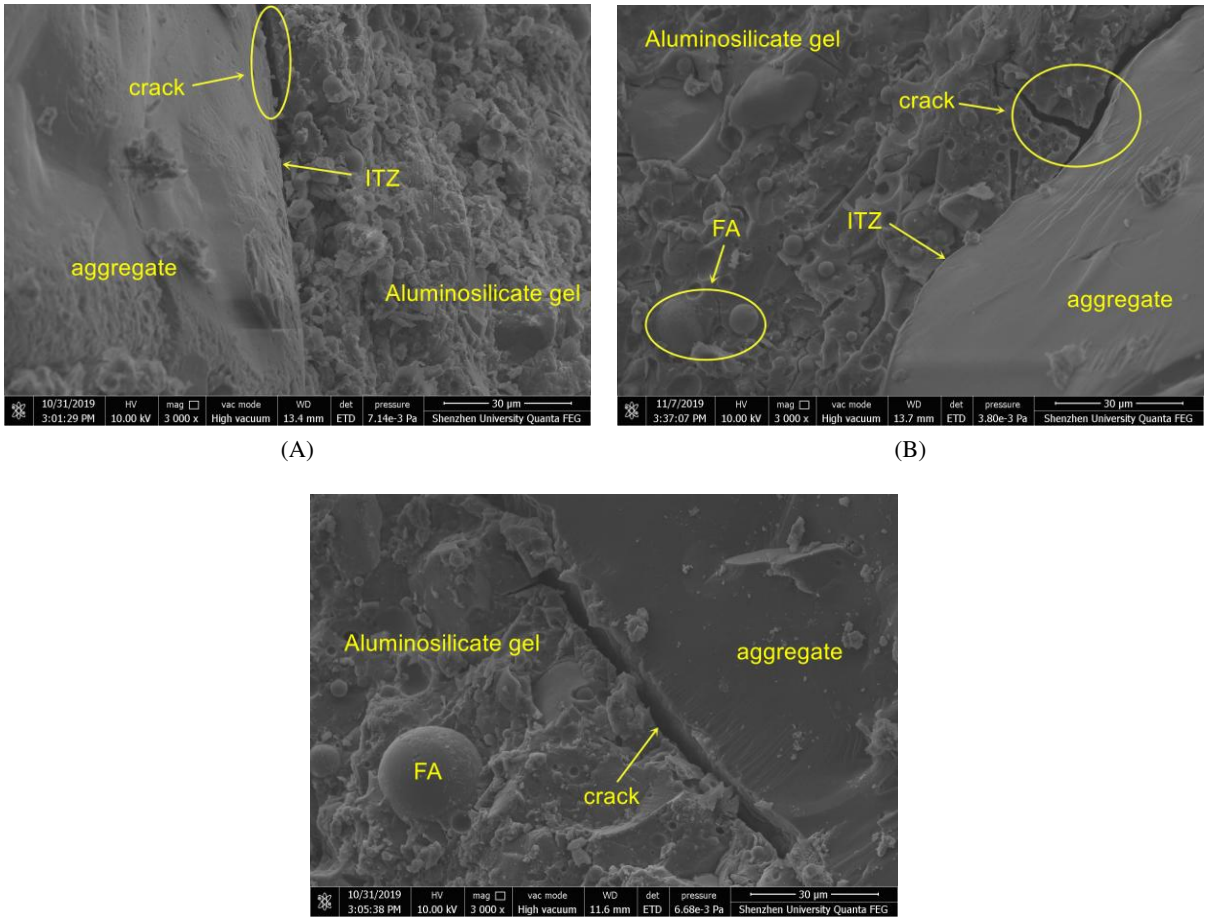

Fig. 14. SEM photos of RS group at 7 days. **(A)** RG-0, **(B)** RG-50, **(C)** RG-100. RS, river sand. ITZ, interface transportation zone; SEM, scanning electron microscopy

ing performance between the GPP and aggregate. Simultaneously, it was found that the bonding performance between the SS–GPC paste and RA is stronger than that of the RS–GPC paste when comparing the ITZ in Figures 13E and 14C. The presence of SS improves the performance of the ITZ between the geopolymer and RA, and eventually leads to a higher compressive strength of SS–GPC than that of RS–GPC with a high RA replacement ratio.

The compressive strengths of SG-0, SG-25, SG-50, SG-75, and SG-100 increased by 37.29%, 38.99%, 41.10%, 41.62%, and 28.52% from 7 days to 28 days, respectively. With an increase in the RA content, microcracks in the aggregate will see the infusion of more water, causing a more alkaline excitation of the hydration reaction of the solvent, which can make the reaction more intense and complete, thus, promoting the development of its late strength. However, the strength loss caused by a defect in the RA is greater at a 100% replacement ratio. The compressive strengths of RG-0, RG-50, and RG-100 increased by 19.38%, 15.92%, and 10.15%, respectively, from 7 days to 28 days. This is mainly because the aggregate is the weak part of the whole specimen, and its strength significantly impacts the overall strength of the specimen, leading to a decrease in the rate of increase in strength with an increase in the RA replacement ratio.

As the bonding force between GPC and aggregate is much higher than that between OPCC and aggregate, making ITZ denser, the compres-

sive strength of GPC was higher than OPCC. At the same time, the compressive strengths of SPC-100 and RG-0 were higher than those of RPC-100 and SG-0, indicating that SS increased the compressive strength of RA-OPCC and decreased that of NA-GPC to some extent.

4.4. Elastic modulus E_c

The influence of the RA replacement ratio and sand type on the elastic modulus (E_c) of the concrete cylinder specimen is shown in Figure 15. It can be seen that the variation rates of the two groups were similar to that of the compressive strength. Observing the curves of the SS–GPC, the effect of the RA replacement ratio on the elastic modulus at 7 days was very small (12% difference between maximum and minimum), while the effect at 28 days increased first and then decreased. By observing the RS–GPC curve, the elastic modulus curves show a significant downward trend with an increase in the RA replacement ratio.

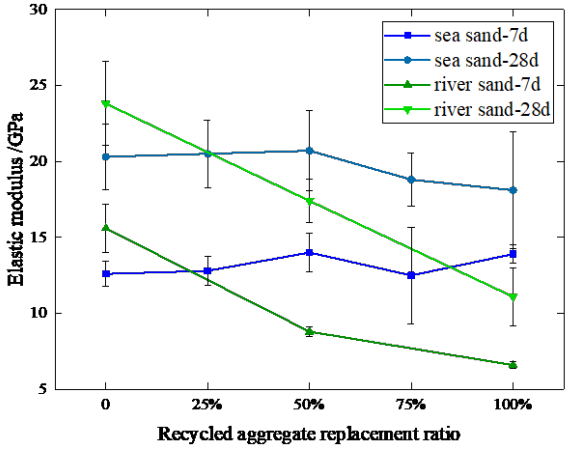

Fig. 15. Influence of RA replacement ratio and sand types on elastic modulus. RA, recycled aggregate

In the SS–GPC, the improvement rates of the elastic modulus from 7 days to 28 days were 61.11%, 60.16%, 47.86%, 50.40%, and 30.22%, respectively, which decreased with an increase in the RA replacement ratio. In the RS–GPC, the improvement rates were 52.56%, 97.73%, and 68.18%, showing a trend of first increasing and then decreasing. However, the elastic modulus of OPCC (SPC-100 and RPC-100) is much higher than that of GPC (SG-100 and RG-100), but the improvement rates were only 5.8% and 4.8%, respectively, which indicates that the elastic modulus of SPC-100 and RPC-100 has matured in the early stage.

4.5. Stress-strain response

Figures 16 and 17 show the complete stress–strain curves of SS–GPC and RS–GPC at 7 days and 28 days, respectively. Figure 18 shows the complete stress–strain curves of GPC and OPCC at 7 days and 28 days under the condition of 100%

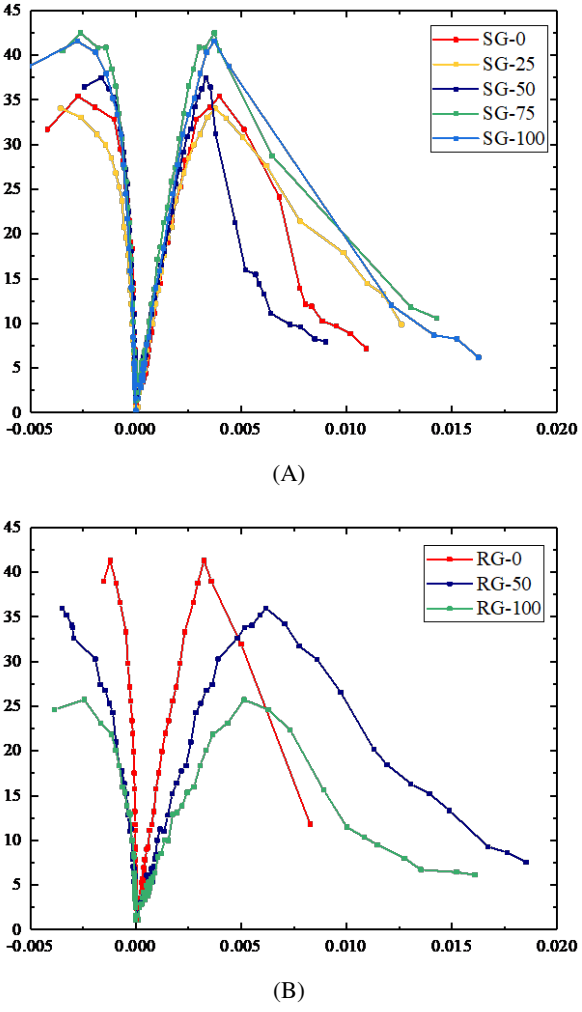

Fig. 16. Stress–strain curves at 7 days. **(A)** SS–GPC, **(B)** RS–GPC. RS–GPC, river sand geopolymer concrete; SS–GPC, sea sand geopolymer concrete

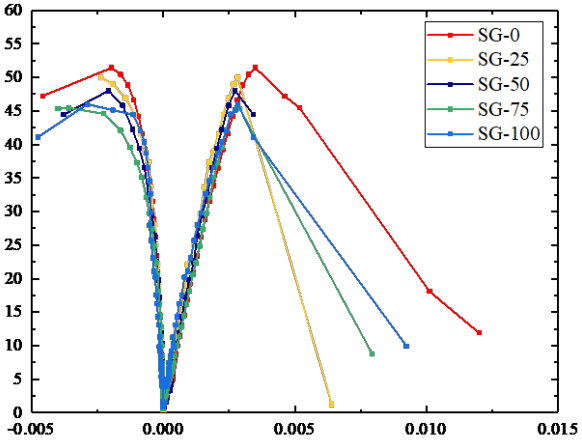

(A)

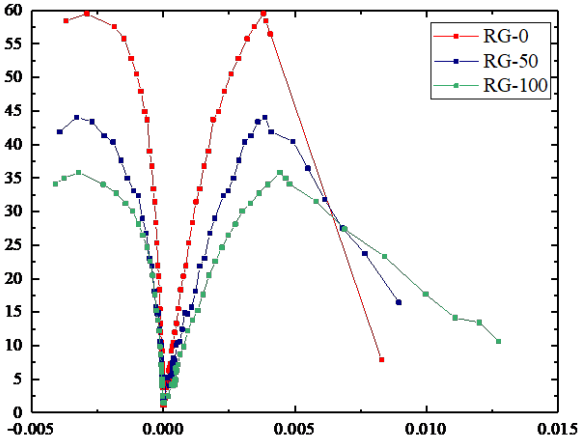

(B)

Fig. 17. Stress–strain curves at 28 days. **(A)** SS–GPC, **(B)** RS–GPC. RS, river sand geopolymer concrete; SS–GPC, sea sand geopolymer concrete

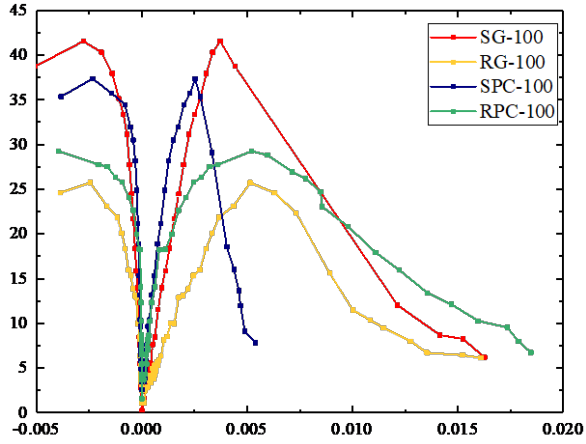

(A)

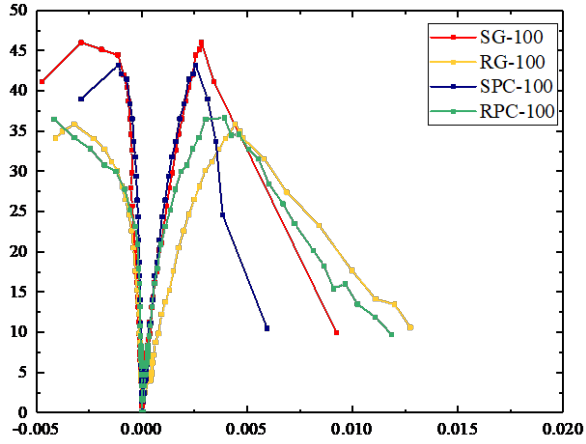

(B)

Fig. 18. Comparison of GPC and ordinary silicate concrete. **(A)** 7 days, **(B)** 28 days. GPC, geopolymer concrete

RA replacement ratio. In all images, the vertical axis represents the stress, the positive X-axis represents the longitudinal strain, and the negative X-axis represents the transverse strain.

In Figures 16 and 17, the change rules of the cylinder compressive strength of the GPC are similar to that of the cube compressive strength. The reason for this rule is similar to that of the cube compressive strength. The rising segments of the longitudinal strain and transverse strain curves of SS–GPC almost coincide completely, indicating that the RA replacement ratio has little effect on the strength and stiffness. It can also be seen that each curve has a considerable decreasing section, where the specimens show ductile failure characteristics at 7 days but brittle failure characteristics at 28 days. In contrast, with an increase in the RA replacement ratio, the slope of the longitudinal strain rising section decreased, but the ductility was enhanced in RS–GPC. The specimens with a higher strength exhibited greater stiffness. At the same time, the transverse strain showed a similar trend.

In Figure 18, the curves of OPCC are steeper than those of GPC. OPCC has a higher stiffness but lower strength compared to GPC, indicating that there is no relationship between stiffness and strength. The use of SS improves the stiffness of

the GPC or OPCC. Over time, the stiffness of the RC group can develop to be similar to that of the SS group (see Figure 18B).

4.6. Other mechanical properties

4.6.1. Splitting tensile strength f_{ct}

In Figure 19, at 7 days, the splitting tensile strength (f_{ct}) of SS–GPC remained relatively stable with an increase in the RA replacement ratio, but it decreased markedly at 28 days; however, in the RS–GPC group, there was a very significant and regular decline. For the SS–GPC, the splitting tensile strengths of SG-25, SG-50, SG-75, and SG-100 increased by 1.61%, 7.26%, 4.84%, and 5.65%, respectively, at 7 days, and decreased by 4.62%, 8.67%, 12.14%, and 16.76%, respectively, at 28 days compared with that of SG-0. For RS–GPC, the splitting tensile strength of RG-50 and RG-100 respectively decreased by 16.7% and 32.1% at 7 days, and 13.3% and 31.8% at 28 days with 50% and 100% RA replacement ratios compared with those of RG-0. These laws and reasons are similar to those of the cube compressive strength, except that the splitting tensile strength of concrete is mainly affected by its crack resistance and tensile strength; therefore, it largely depends on the ITZ strength. The ITZ strength between the old mortar attached to the RA surface and the new mortar is much lower than that between the NA and the new mortar [38]; therefore, the adverse effect of RA due to its own defects on the splitting tensile strength is more obvious than that on the compressive strength. With an increase in the RA replacement ratio, the splitting tensile strength decreased more than the compressive strength.

For SS–GPC, the 28 days strength improvement rates were 39.52%, 30.95%, 18.80%, 16.92%, and 9.92% for SG-0, SG-25, SG-50, SG-75, and SG-100, respectively, showing a gradually decreasing trend. With the increase in the RA replacement ratio, the 28 days strength considerably decreases while the 7 days strength is basically unchanged. For RS–GPC, the 28 days strength improvement rates were 6.13%, 11.11%, and 7.27% for RG-0, RG-50, and RG-100, respectively, showing a small fluctuation. This is because the specimens had started to become destroyed from the ITZ or RA irrespective of the curing period.

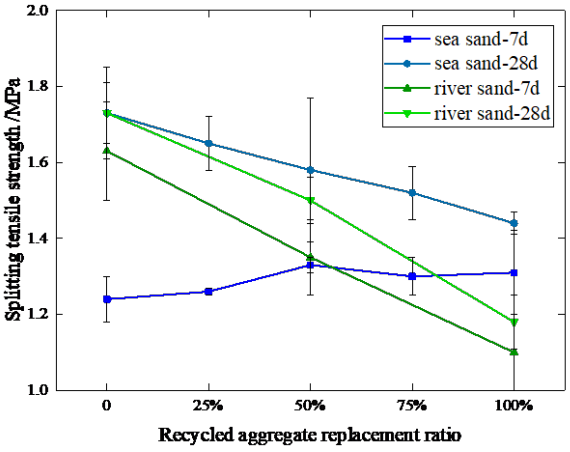

Fig. 19. Influence of RA replacement ratio and sand types on splitting tensile strength. RA, recycled aggregate

4.6.2. Flexural strength $f_{ct,f}$

Similar to the splitting tensile strength, the flexural strength ($f_{ct,f}$) is also affected by the crack resistance and tensile strength of concrete, making the overall variation in flexural strength similar to the splitting tensile strength.

In Figure 20, the flexural strength of SS–GPC remained relatively stable with the increase in RA replacement ratio at 7 days, but it significantly decreased at 28 days. However, in the RS–GPC group, there was a considerably regular decline, and the decline at 28 days was more significant than that at 7 days. The improvement rates from 7 days to 28 days were 38.59%, 27.69%, 26.20%, 22.51%, and 20.13% in SS–GPC and 24.17%, 11.32%, and 8.12% in RS–GPC. In contrast to the compressive strength and splitting tensile strength, the improvement rates of the flexural strength from 7 days to 28 days decreased in SS–GPC and RS–GPC with the increase in the RA replacement ratio, indicating that the loss of flexural strength caused by RA is greater.

As listed in Table 9, the splitting tensile strength and flexural strength of SPC-100 and RPC-100 are higher than those of SG-100 and RG-100, despite the compressive strength of OPCC being lower

than that of GPC. This may be related to the 3D layered structure of GPC, which can withstand a higher pressure but has a lower tensile strength.

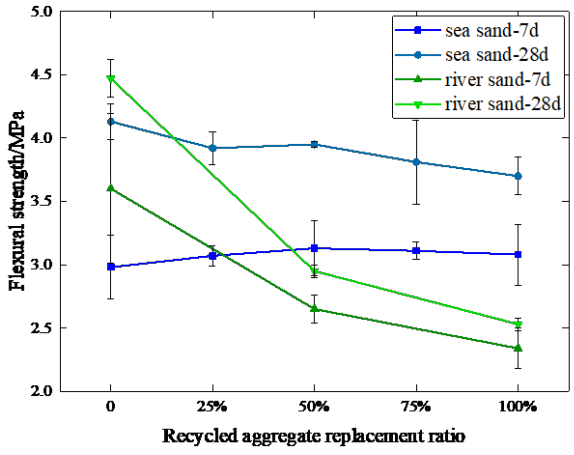

Fig. 20. Influence of RA replacement ratio and sand types on flexural strength. RA, recycled aggregate

4.6.3. Poisson's ratio μ

There is no exact relationship between μ and the RA replacement ratio. The Poisson's ratio shows a fluctuating trend with an increase in the RA replacement ratio.

5. Conclusions

In this study, after determining the optimum mix proportions of slurry using the orthogonal array test, the influence of the RA replacement ratio (0% 25%, 50%, 75%, and 100%) and the type of sand (SS and RS) on the working performance and basic mechanical properties of GPC was studied. Within the scope of this paper, the following conclusions were made:

1. The optimum mix proportions of the slurry are 12 mol/L NaOH solution concentration, 30% slag content, and 0.3 water-binder ratio.
2. In the early stage, seawater and SS hindered the hydration reaction of the geopolymer to a certain extent and reduced the early compressive strength of the GPC slurry. However, the blocking effect becomes less significant or even negligible in the later stages.
3. The cube compressive strength of SS–GPC shows little change with the RA replacement ratio, but it shows a considerable and regular downward trend in RS–GPC. The reason for this is that the weak point of SS–GPC in the early stage lies in the matrix rather than the aggregate, and in the later stage, it gradually transfers to ITZ and RA with an increase in the RA replacement ratio; the weak point of RS–GPC is always ITZ and RA owing to the higher strength of the RS–GPC matrix. The same phenomenon was observed in the splitting tensile strength and flexural strength tests.
4. The bonding strength of GPC was much stronger than that of OPCC. In GPC, the ITZ is no longer the weakest part, so the strength of the aggregate can be fully exerted.
5. The elastic modulus of SS–GPC shows little change with an increase in the RA replacement ratio, but it shows a significant decreasing trend in the RS–GPC. There is a certain degree of correlation between the compressive strength and elastic modulus of the GPC.
6. It is known from this paper that a certain reaction in seawater and SS hinders the early hydration reaction of geopolymers and thus reduces the early strength. However, further research is needed to fully identify the explicit factor for this to happen.
7. This paper focuses on the microstructural and mechanical properties of GC. The durability, fire resistance, and other properties still need to be studied.

CRediT authorship contribution statement

All authors contributed to the study conception and design. W.L.: Data acquisition, Methodology, Formal analysis, Supervision, and editing. X.H.: Conceptualization, Methodology, Investigation, Formal analysis, Visualization, writing – original draft. J.Z., and E.S.D.: Data analysis, Writing – review and Visualization, Y.H., and X.Y.: Visualization and editing. All authors read and approved the final manuscript.

Declaration of Conflict of Interest

The authors declare that they have no competing conflict of interest.

Acknowledgements

The authors appreciate the financial support provided by the National Natural Science Foundation of China (NSFC Grant Numbers: 51878415, 51908373). Technical support is acknowledged from Guangdong Provincial Key Laboratory of Durability for Marine Civil Engineering (SZU), No. 2020B1212060074.

References

[1] Gartner E. Industrially interesting approaches to "low-CO_2" cements. Cem Concr Res. 2004;34(9):1489–98. https://doi.org/10.1016/j.cemconres.2004.01.021

[2] Peng JX, Huang L, Zhao Y, Chen P, Zeng L, Zheng W. Modeling of carbon dioxide measurement on cement plants. Adv Mater Res. 2012;610–613:2120–8. https://doi.org/10.4028/www.scientific.net/AMR.610-613.2120

[3] Hardjito D, Wallah SE, Sumajouw DMJ, Rangan BV. Fly ash-based geopolymer concrete. Aust J Struct Eng. 2005; 6(1):77–86. https://doi.org/10.1080/13287982.2005.11464946

[4] Singh B, Ishwarya G, Gupta M, Bhattacharyya SK. Geopolymer concrete: a review of some recent developments. Constr Build Mater. 2015;85:78–90. https://doi.org/10.1016/j.conbuildmat.2015.03.036

[5] Mangi SA, Makhija A, Raza MS, Khahro SH, Jhatial AA. A comprehensive review on effects of seawater on engineering properties of concrete. Silicon. 2021;13(12):4519–26. https://doi.org/10.1007/s12633-020-00724-7

[6] Vargas A, Dal Molin DCC, Vilela ACF, da Silva FJ, Pavão B, Veit H. The effects of Na2O/SiO2molar ratio, curing temperature and age on compressive strength, morphology and microstructure of alkali-activated fly ash-based geopolymers. Cem Concr Compos. 2011;33(6):653–60. https://doi.org/10.1016/j.cemconcomp.2011.03.006

[7] Yip CK, Lukey GC, Provis JL, van Deventer JSJ. Effect of calcium silicate sources on geopolymerisation. Cem Concr Res. 2008;38(4):554–64. https://doi.org/10.1016/j.cemconres.2007.11.001

[8] Ismail I, Bernal SA, Provis JL, San Nicolas R, Hamdan S, van Deventer JSJ. Modification of phase evolution in alkali-activated blast furnace slag by the incorporation of fly ash. Cem Concr Compos. 2014;45:125–35. https://doi.org/10.1016/j.cemconcomp.2013.09.006

[9] Morsy MS, Alsayed SH, Al-Salloum Y, Almusallam T. Effect of sodium silicate to sodium hydroxide ratios on strength and microstructure of fly ash geopolymer binder. Arab J Sci Eng. 2014;39(6):4333–9. https://doi.org/10.1007/s13369-014-1093-8

[10] Hasnaoui A, Ghorbel E, Wardeh G. Performance of metakaolin/slag-based geopolymer concrete made with recycled fine and coarse aggregates. J Build Eng. 2021;42:102813. https://doi.org/10.1016/j.jobe.2021.102813

[11] Xiao J, Qiang C, Nanni A, Zhang K. Use of sea-sand and seawater in concrete construction: current status and future opportunities. Constr Build Mater. 2017;155:1101–11. https://doi.org/10.1016/j.conbuildmat.2017.08.130

[12] Nuaklong P, Sata V, Chindaprasirt P. Influence of recycled aggregate on fly ash geopolymer concrete properties. J Clean Prod. 2016;112:2300–07. https://doi.org/10.1016/j.jclepro.2015.10.109

[13] Le HB, Bui QB, Tang L. Geopolymer recycled aggregate concrete: from experiments to empirical models. Materials. 2021;14(5):1180. https://doi.org/10.3390/ma14051180

[14] Nuaklong P, Wongsa A, Boonserm K, Ngohpok C, Jongvivatsakul P, Sata V, et al. Enhancement of mechanical properties of fly ash geopolymer containing fine recycled concrete aggregate with micro carbon fiber. J Build Eng. 2021;41:102403. https://doi.org/10.1016/j.jobe.2021.102403

[15] Kotop MA, El-Feky MS, Alharbi YR, Abadel AA, Binyahya AS. Engineering properties of geopolymer concrete incorporating hybrid nano-materials. Ain Shams Eng J. 2021;12(4):3641–47. https://doi.org/10.1016/j.asej.2021.04.022

[16] Xiao J, Li W, Fan Y, Huang X. An overview of study on recycled aggregate concrete in China (1996–2011). Constr Build Mater. 2012;31:364–83. https://doi.org/10.1016/j.conbuildmat.2011.12.074

[17] Silva RV, de Brito J, Dhir RK. Establishing a relationship between modulus of elasticity and compressive strength of recycled aggregate concrete. J Clean Prod. 2016;112:2171–86. https://doi.org/10.1016/j.jclepro.2015.10.064

[18] Li W, Luo Z, Long C, Wu C, Duan WH, Shah SP. Effects of nanoparticle on the dynamic behaviors of recycled aggregate concrete under impact loading. Mater Des. 2016;112:58–66. https://doi.org/10.1016/j.matdes.2016.09.045

[19] Kisku N, Joshi H, Ansari M, Panda SK, Nayak S, Dutta SC. A critical review and assessment for usage of recycled aggregate as sustainable construction material. Constr Build Mater. 2017;131:721–40. https://doi.org/10.1016/j.conbuildmat.2016.11.029

[20] Shi XS, Collins FG, Zhao XL, Wang QY. Mechanical properties and microstructure analysis of fly ash geopolymeric recycled concrete. J Hazard Mater. 2012;237–238:20–9. https://doi.org/10.1016/j.jhazmat.2012.07.070

[21] Khedmati M, Kim YR, Turner JA. Investigation of the interphase between recycled aggregates and cementitious binding materials using integrated microstructural-nanomechanical-chemical characterization. Compos

Part B. 2019;158:218–29. https://doi.org/10.1016/j.compositesb.2018.09.041

[22] Olivia M, Nikraz H. Properties of fly ash geopolymer concrete designed by Taguchi method. Mater Des (1980–2015). 2012;36:191–8. https://doi.org/10.1016/j.matdes.2011.10.036

[23] Mehta A, Siddique R, Singh BP, Aggoun S, Łagód G, Barnat-Hunek D. Influence of various parameters on strength and absorption properties of fly ash based geopolymer concrete designed by Taguchi method. Constr Build Mater. 2017;150:817–24. https://doi.org/10.1016/j.conbuildmat.2017.06.066

[24] Cao YF, Tao Z, Pan Z, Wuhrer R. Effect of calcium aluminate cement on geopolymer concrete cured at ambient temperature. Constr Build Mater. 2018;191:242–52. https://doi.org/10.1016/j.conbuildmat.2018.09.204

[25] Hu Y, Tang Z, Li W, Li Y, Tam VWY. Physical-mechanical properties of fly ash/GGBFS geopolymer composites with recycled aggregates. Constr Build Mater. 2019;226:139–51. https://doi.org/10.1016/j.conbuildmat.2019.07.211

[26] Xie J, Wang J, Rao R, Wang C, Fang C. Effects of combined usage of GGBS and fly ash on workability and mechanical properties of alkali activated geopolymer concrete with recycled aggregate. Compos Part B. 2019;164:179–90. https://doi.org/10.1016/j.compositesb.2018.11.067

[27] ASTM C469/C469M. Test method for static modulus of elasticity and poissons ratio of concrete in compression. ASTM Int. 2014; https://doi.org/10.1520/C0469_C0469M-14E01

[28] Nuaklong P, Sata V, Chindaprasirt P. Properties of metakaolin-high calcium fly ash geopolymer concrete containing recycled aggregate from crushed concrete specimens. Constr Build Mater. 2018;161:365–73. https://doi.org/10.1016/j.conbuildmat.2017.11.152

[29] Poon CS, Shui ZH, Lam L, Fok H, Kou SC. Influence of moisture states of natural and recycled aggregates on the slump and compressive strength of concrete. Cem Concr Res. 2004;34(1):31–6. https://doi.org/10.1016/S0008-8846(03)00186-8

[30] Behera M, Bhattacharyya SK, Minocha AK, Deoliya R, Maiti S. Recycled aggregate from C&D waste & its use in concrete – A breakthrough towards sustainability in construction sector: a review. Constr Build Mater. 2014;68:501–16. https://doi.org/10.1016/j.conbuildmat.2014.07.003

[31] Xie J, Wang J, Zhang B, Fang C, Li L. Physicochemical properties of alkali activated GGBS and fly ash geopolymeric recycled concrete. Constr Build Mater. 2019;204:384–98. https://doi.org/10.1016/j.conbuildmat.2019.01.191

[32] Shaikh FUA. Mechanical and durability properties of fly ash geopolymer concrete containing recycled coarse aggregates. Int J Sustain Built Environ. 2016;5(2):277–87. https://doi.org/10.1016/j.ijsbe.2016.05.009

[33] Ali B, Gulzar MA, Raza A. Effect of sulfate activation of fly ash on mechanical and durability properties of recycled aggregate concrete. Constr Build Mater. 2021;277:122329. https://doi.org/10.1016/j.conbuildmat.2021.122329

[34] Shi C, Li Y, Zhang J, Li W, Chong L, Xie Z. Performance enhancement of recycled concrete aggregate – A review. J Clean Prod. 2016;112:466–72. https://doi.org/10.1016/j.jclepro.2015.08.057

[35] Alhazmi H, Shah S, Mahmood A. Sustainable development of innovative green construction materials: a study for economical eco-friendly recycled aggregate based geopolymer concrete. Materials. 2020;13(21):4881. https://doi.org/10.3390/ma13214881

[36] Xu Z, Huang Z, Liu C, Deng X, Hui D, Deng S. Research progress on mechanical properties of geopolymer recycled aggregate concrete. Rev Adv Mater Sci. 2021;60(1):158–72. https://doi.org/10.1515/rams-2021-0021

[37] Nguyen KT, Le TA, Lee K. Evaluation of the mechanical properties of sea sand-based geopolymer concrete and the corrosion of embedded steel bar. Constr Build Mater. 2018;169:462–72. https://doi.org/10.1016/j.conbuildmat.2018.02.169

[38] Saradar A, Tahmouresi B, Mohseni E, Shadmani A. Restrained shrinkage cracking of fiber-reinforced high-strength concrete. Fibers. 2018;6(1):12. https://doi.org/10.3390/fib6010012

[39] Posi P, Teerachanwit C, Tanutong C, Limkamoltip S, Lertnimoolchai S, Sata V, et al. Lightweight geopolymer concrete containing aggregate from recycle lightweight block. Mater Des (1980–2015). 2013;52:580–6. https://doi.org/10.1016/j.matdes.2013.06.001

[40] Sata V, Wongsa A, Chindaprasirt P. Properties of pervious geopolymer concrete using recycled aggregates. Constr Build Mater. 2013;42:33–9. https://doi.org/10.1016/j.conbuildmat.2012.12.046

Received 2022-01-23
Accepted 2022-02-20